Latin American Journal of Solids and Structures
www.lajss.org

Influence of slab length on dynamic characteristics of subway train-steel spring floating slab track-tunnel coupled system

Abstract

A subway train-steel spring floating slab track-tunnel coupling dynamic model, considering short and middle-long wavelength random track irregularities, and longitudinal connection between adjacent slabs of steel spring floating slab track, was developed. And the influence of slab length on dynamic characteristics of the system under different track conditions and train speeds are theoretically studied. The calculated results show: (1) In general, the acceleration of each component of the coupled system decreases with the increase of slab length under the perfectly smooth track condition; (2) Slab length has different influence laws on acceleration of each component of subway train-steel spring floating slab track-tunnel coupled system under random irregularity of track condition. The lower the dominant frequency distribution of vibration acceleration is, the higher influence slab length has; (3) With the increase of slab length, the force of rail, fastener and steel spring also decreases significantly, which helps to lengthen the service life of these components; (4) With the increase of slab length, the longitudinal bending moment of slab increases sharply at first, then it begins to drop slightly. When slab length exceeds the distance between two bogies of a vehicle, the longitudinal bending moment of slab changes little; (5) Slab length has significant influence on the dynamic force and displacement of the coupled system when train speed is higher.

Keywords

Steel spring; floating slab track; slab length; subway train; dynamic characteristics; tunnel.

Qing-yuan Xu [a,b,c]
Bin Yan [a]
Ping Lou [a,b,c*]
Xiao-lin Zhou[a]

[a] School of Civil Engineering, Railway Campus, Central South University, Changsha, Hunan 410075, China.
[b]Key Laboratory of Heavy Railway Engineering Structure of Education Ministry, Railway Campus, Central South University, Hunan 410075, China.
[c] Collaborative Innovation Center of Rail Safety, Central South University, Hunan 410075, China.

Corresponding author email:
*pinglou@csu.edu.cn

http://dx.doi.org/10.1590/1679-78251327

Received 05.05.2014
In revised form 22.09.2014
Accepted 22.09.2014
Available online 13.10.2014

1 INTRODUCTION

Urban rail transit has been widely used owing to its large capacity, punctuality, safety, reliability, and comfortable passenger environment. However, this mode of transportation is also accompanied by an environmental vibration problem due to the operation of subway trains. A variety of vibra-

tion-reduction measures have been undertaken during the design and construction of subway lines. Among them, the floating slab track (FST) structure has been widely used for its excellent vibration-reduction capability. Many scholars have conducted extensive research on the FST structure and its impact on environmental vibration.

Hussein and Hunt (2006) studied the dynamic characteristics of a continuous FST on a rigid foundation with moving harmonic loads by the Fourier transform method, and found little difference between static and dynamic calculation results of the continuous FST structure at normal train speeds if the track was perfectly smooth. Using the semi-analytical pipe-in-pipe (PiP) three-dimensional (3D) model to simulate the interaction between a tunnel and a semi-infinite soil foundation, Hussein and Hunt (2009) compared the displacements at the free surface under moving harmonic loads for a track with a discontinuous slab to those for a track with a continuous floating slab.

By means of a 3D numerical model for the prediction of railway induced vibrations that fully accounts for the interaction among the train, the track and the soil, Lombaert et al. (2006) dealt with the effectiveness of a FST for the control of ground-borne vibrations generated by rail transportation systems.

Gupta et al. (2007) compared the semi-analytical PiP 3D model with the coupled periodic finite element-boundary element model, for predicting vibrations due to underground railway traffic, and the effect of coupling a floating slab to the tunnel – soil system is studied with both models by calculating the insertion gain. With the coupled periodic finite element-boundary element model, Gupta et al. (2008) studied the effect of environmental vibration induced by the metro traffic of Beijing subway line 4 on the equipment of the physics laboratory of Beijing University; Gupta and Degrande (2010) used the model to assess the vibration isolation efficiency of continuous and discontinuous floating slab tracks.

Kuo et al. (2008) developed a vehicle-FST coupling dynamic model on a rigid foundation, and studied the influence of train speed, floating slab stiffness, floating slab mass, and fastener stiffness on the dynamic characteristics of the FST structure.

Taking the nonlinear suspension stiffness of the vehicle into account, Müller et al. (2008) developed a train-FST-tunnel-soil coupling dynamic model, and studied the influence of nonlinear vehicle suspension stiffness and equivalent linear vehicle suspension stiffness on the dynamic characteristics of the coupled system.

Auersch (2012) analyzed the dynamics of slab track and FST for a great variety of track and soil parameters by multibeam models for the track and by integration in the wave-number domain for the soil, which is modeled as a layered half-space. The reduction effects of the FST are examined and compared with the reduction of the ground vibration away from the railway line.

In order to protect the cultural receptors along the Athens metro extension to Piraeus due to ground borne noise and vibration, Vogiatzis (2012) numerically predicted the ground borne noise and vibration levels for sensitive buildings along the metro extension with standard STEDEF track and FST respectively, and compared the prediction results with the allowable ground borne noise and vibration level. The installation of floating slab in some special sections was suggested.

Recently, Hung et al. (2013) incorporated the railway irregularity and dynamic properties of the moving train in a 2.5D finite/infinite-element prediction model to study the effect of railway irregularity on soil vibrations due to moving trains.

In addition to theoretical researches, numerous experimental studies have also been performed regarding the dynamic characteristics of FST and their effects on environmental vibration. At the Laboratory of Track Vibration Abatement and Control, which is an underground facility of Beijing Jiaotong University in China, Ding et al. (2011) applied harmonic loads with frequencies of 5-16 Hz on FST with different stiffness and supporting spacing, and measured the vibration responses of the FST, the underground tunnel, and the free ground surface at distances 0-80 m away from the underground tunnel. Saurenman and Phillips (2006) conducted an environmental vibration test near one section of a FST of the BART rapid line. Cox et al. (2006) built a 2.5-meter-long full-scale FST model in an indoor laboratory, applied harmonic loads of different frequencies on the rail, and measured the vibration characteristics of the FST structure.

As can be seen from the above description, many theoretical and experimental research efforts have been made on the dynamic characteristics of FST and their influence on environmental vibration. However, few studies have been made on the influence of slab length, which is a key technical parameter of FST structure, on the dynamic characteristics of the subway train-FST-tunnel-soil coupled system.

The remaining of this paper is organized as follows. At first, a subway train-steel spring floating slab track (SSFST)-tunnel coupling dynamic model that considers both short and middle to long wavelength random track irregularities, the longitudinal connection between adjacent slabs of SSFST and the coupling effect of the entire system is developed. And then corresponding computer programs are compiled to study the influence of slab length on the dynamic characteristics of the coupled system under different track irregularity conditions and train speeds.

2 COUPLING DYNAMIC MODEL

A schematic describing the dynamic model for a subway train traveling on a FST in a tunnel at a constant speed v along the longitudinal direction is shown in Figure 1.

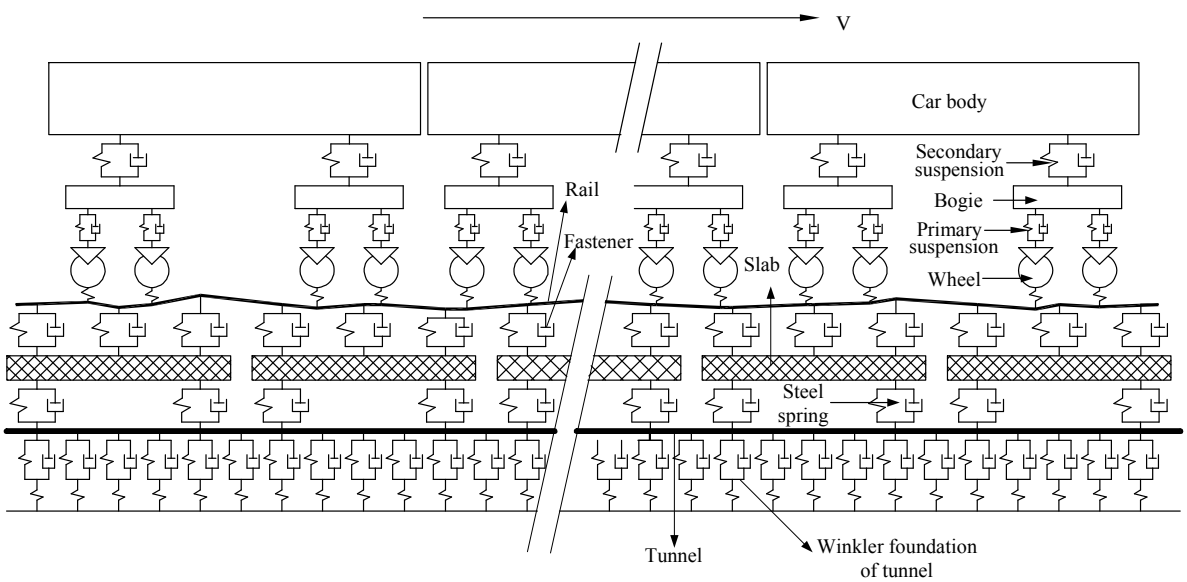

Figure 1: Schematic of the coupling dynamic model.

The model consists of four sub-models, namely, the subway train, the SSFST-tunnel, wheel-rail interaction, and track irregularity sub-models. They are explained as follows.

2.1 Subway train sub-model

As shown in Figure 1, the subway train sub-model consists of a series of identical four-wheel vehicles. Each vehicle in the train is modeled as a mass-spring-damper system consisting of a car body with vertical and pitch motions, two bogie frames with vertical and pitch motions, four wheels with vertical motions, and two-stage suspensions. Therefore, each vehicle has 10 degrees of freedom (DOFs).

2.2 SSFST-tunnel sub-model

The SSFST-tunnel is a spatial structure. The sub-model can reflect the spatial dynamic characteristics of a SSFST-tunnel-soil system well using volume elements with a small mesh size to simulate the slab, tunnel, and surrounding soil. However, calculations are very time-consuming if volume elements with a small mesh size are used, especially in this study. The reasons are as follows.

Firstly, as shown in Figure 2, to eliminate the influence of boundary conditions, more than 20 m of track to the left and right sides upon which the train does not travel must be included. In addition, the actual length of the train (6 vehicles, 114 m) and a long moving distance of train (330 m) are considered. Therefore, the total length of the dynamic model is more than 500 m, which results in a large number of DOFs to simulate the coupled system.

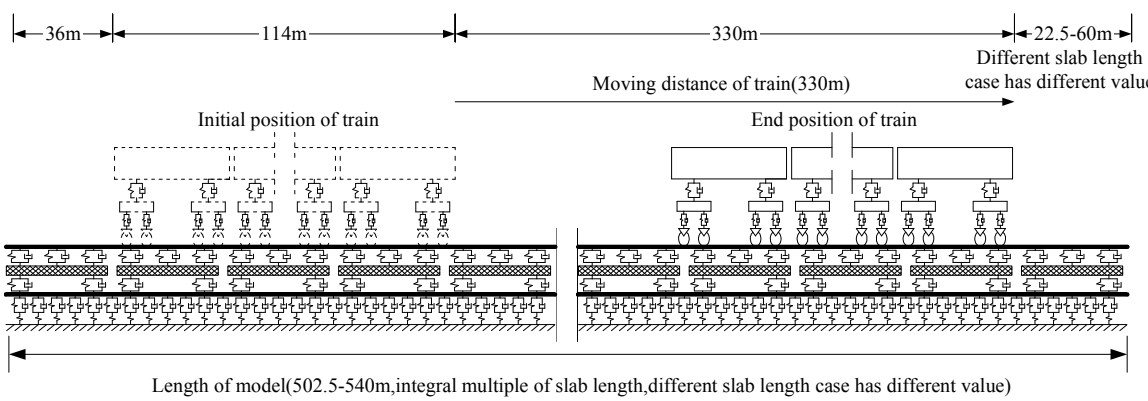

Figure 2: Layout of train and track.

Secondly, to appropriately include the influence of short wavelength random track irregularity, the train moving distance during each time step should be less than half of the minimum wavelength of the track irregularity considered. As a result, a very small time step is required in the simulation.

Finally, the dynamic force of the components of the FST is very sensitive to the finite element size. To obtain a reasonable value for the dynamic force, the finite element mesh size should be

sufficiently small. A small finite element size is also required in this study to reasonably simulate the continuous support characteristics of the tunnel.

For the reasons given above, it is extremely time-consuming if small mesh size volume elements are used to simulate the slab, the tunnel, and surrounding soil, and the calculations are not easily conducted on an ordinary personal computer at present. To reduce the calculation time, according to reference (Gardien and Stuit, 2003), a long beam supported on a Winkler elastic foundation is used to model the tunnel. The SSFST-tunnel sub-model is shown in Figure 3.

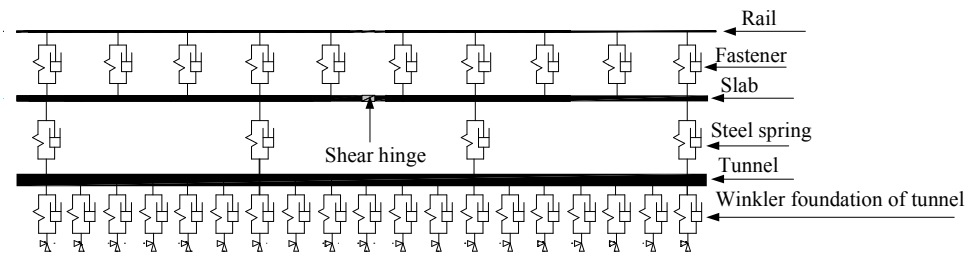

Figure 3: SSFST-tunnel dynamic model.

The rail, slab, and tunnel are simulated by Bernoulli-Euler beam elements, while fasteners which connect rail and slab, steel springs which connect slab and tunnel, shear hinges which connect two adjacent slabs, as well as the Winkler foundation of the tunnel are simulated by linear spring-damper elements.

A sophisticated 3D SSFST-tunnel-soil model (Figure 4) is used to determine the equivalent stiffness of the Winkler foundation of the tunnel. In the model, the rail is simulated by Bernoulli-Euler beam elements. The slab, tunnel, soil, and steel spring are simulated by volume elements. Fasteners and shear hinges are simulated by linear spring-damper elements.

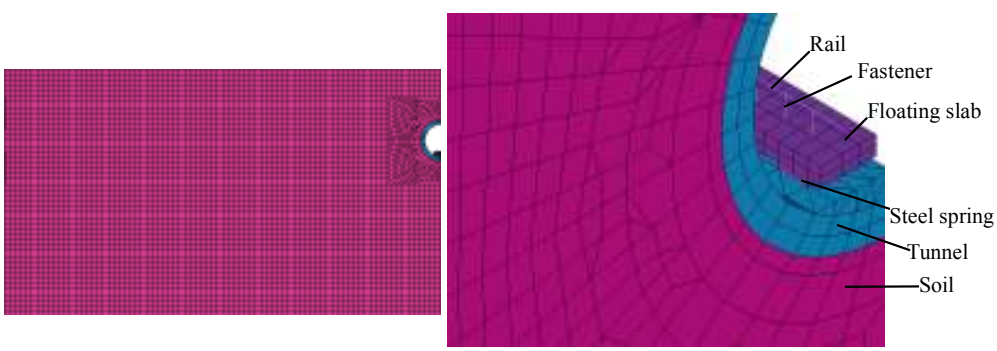

Figure 4: Sophisticated 3D SSFST-tunnel-soil model.

The procedures used to determine the equivalent stiffness of the Winkler foundation of the tunnel (Figure 3) are as follows.

(1) Use ANSYS Parametric Design Language to develop the SSFST-tunnel model (Figure 3) and the sophisticated 3D SSFST-tunnel-soil model (Figure 4).

(2) Apply the train load to the sophisticated 3D SSFST-tunnel-soil model (Figure 4), and obtain the maximum vertical displacement y of the tunnel.

(3) Three initial values for the stiffness of the Winkler foundation of the tunnel are assumed. The value of the first initial stiffness k_1 is a small value that is much less than the calculated equivalent stiffness of the Winkler foundation of the tunnel; the value of the second initial stiffness k_2 is a large value that is much larger than the calculated equivalent stiffness of the Winkler foundation of the tunnel; and the value of the third initial stiffness k_3 is the average stiffness of k_1 and k_2.

(4) Apply the train load to the SSFST-tunnel model (Figure 3) with Winkler foundation stiffness values k_1, k_2, and k_3, and obtain the maximum vertical displacements of the tunnel y_1, y_2, and y_3, respectively.

(5) Calculate the error between y and y_3. If the error between y and y_3 is less than 1×10^{-9} m, then the calculated equivalent stiffness of the Winkler foundation of the tunnel is k_3. Otherwise, return to procedure (4) and continue the computation using the bi-section iterative method until the relative error between y and y_3 is less than 1×10^{-9} m.

2.3 Wheel-rail interaction model

The wheel-rail interaction model is shown in Figure 5. The interaction between the wheel and the rail is simulated by the moving nonlinear spring element. When the wheel moves forward, the contact point between the wheel and the rail changes constantly.

The vertical force between the wheel and rail can be determined according to the Hertz nonlinear contact theory that considers the track irregularity (Zhai and Cai, 1997; Lei and Noda, 2002) as follow:

$$P_j(\mathrm{t}) = \begin{cases} \{\dfrac{1}{G}[Z_w(j,t) - Z_r(j,t) - Z_0(t)]\}^{3/2} & Z_w(j,t) - Z_r(j,t) - Z_0(t) > 0 \\ 0 & Z_w(j,t) - Z_r(j,t) - Z_0(t) \le 0 \end{cases} \tag{1}$$

where $P_j(t)$ is the wheel-rail contact force under the jth wheel at time t; G is the wheel-rail contact constant, $G = 3.86R^{-0.115}\times10^{-8}\mathrm{m/N^{2/3}}$, R is the wheel radius; $Z_{\mathrm{w}}(j,\ t)$ is the displacement of the jth wheel at time t, $Z_{\mathrm{r}}(j,\ t)$ is the rail displacement under the jth wheel at time t, and $Z_0(t)$ is the track irregularity under the jth wheel at time t. $Z_{\mathrm{r}}(j,\ t)$ and $Z_0(t)$ can be determinted according to the coordinate of jth wheel at time t. The detailed procedures to determinte $Z_{\mathrm{r}}(j,\ t)$ and $Z_0(t)$ are as follows:

Assuming that the initial position of the jth wheel of subway train is x_0, and the constant speed of the subway train is V. Then the coordinate of jth wheel is $x_0 + Vt$ at time t. According to the coordinate of jth wheel at time t, the rail element number contacting with the jth wheel at time t, the left node number I of the rail element, the right node number J of the rail element, and the distance between the rail node I and the contacting point of jth wheel can be determined (Figure 5). Assuming that the vertical displacement and rotation displacement of rail node I and node J are v_I, θ_I and v_J, θ_J respectively at time t, the distance between the rail node I and the contacting point of jth wheel is x, the length of rail element is l. The rail displacement

under the jth wheel at time t can be obtained according to shape function of beam element (Bowe and Mullarkey, 2005), which is calculated as follow:

$$Z_r(j,t) = \left(1 - 3\left(\frac{x}{l}\right)^2 + 2\left(\frac{x}{l}\right)^3\right)v_I + \left(x - \frac{2x^2}{l} + \frac{x^3}{l^2}\right)\theta_i + \left(3\left(\frac{x}{l}\right)^2 - 2\left(\frac{x}{l}\right)^3\right)v_j + \left(\frac{-x^2}{l} + \frac{x^3}{l^2}\right)\theta_j \quad (2)$$

Similarly, according to coordinate of jth wheel at time t and sample of random irregularity of track, we can obtain the value of irregularity of track $Z_0(t)$ at the contacting point between the jth wheel and rail at time t.

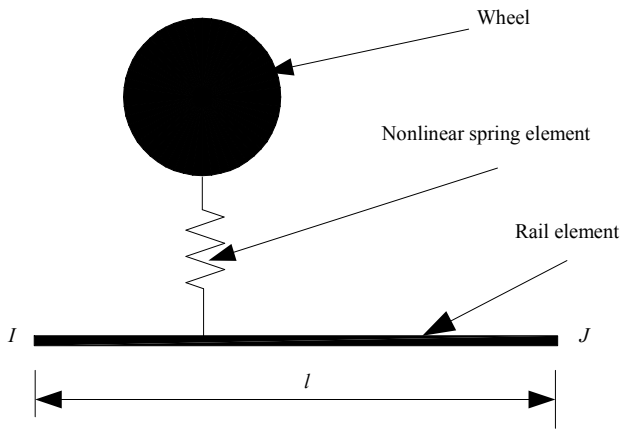

Figure 5: Wheel-rail interaction model.

2.4 Track irregularity model and its sample waves generated in time series

Generally, the track irregularity can be regarded as stationary ergodic Gaussian random processes characterized by power spectral density (PSD) functions. Several PSD curves (Sato, 1977; Hamid and Yang, 1981; Iyengar and Jaiswal, 1995; Dings and Dittrich, 1996; Andersson et al., 1998; Wu and Thompson, 2000; Forrest and Hunt, 2006; Kitagawa and Thompson, 2006), which are given in various empirical forms to describe track irregularity, are available. Among them, PSD curves devised by the Federal Railroad Administration (FRA) of America are widely used in the world (Hamid and Yang, 1981; Lei and Noda, 2002; Au et al., 2002; Gupta et al., 2008; Gupta and Degrande, 2010; Ju et al., 2010; Hung et al., 2013; Zhang and Xia, 2013).

Depending on the irregularities, the track is divided into six classes, Class 6 being the best and Class 1 being the poorest. The expression of the PSD of American track irregularity in the vertical direction is as follow:

$$S(\Omega) = \frac{kA_v{\Omega_c}^2}{\Omega^2(\Omega^2 + {\Omega_c}^2)} \quad (3)$$

where $S(\Omega)$ is the power spectral density of track irregularity, Ω is the spatial frequency in rad/m, k is a constant value of 0.25, Ω_c is a constant value of 0.8245 rad/m, and A_v is a coefficient associated with the class of track, as shown in Table 1.

Class of track	A_v (cm^2/rad/m)
6	0.0339
5	0.2095
4	0.5376
3	0.6816
2	1.0181
1	1.2107

Table 1: Coefficients for A_v.

The PSD of American Class 6 track irregularity, which has been widely used in studies of vibrations generated by underground subway trains, is used to simulate the middle to long wavelength (greater than 1 m) random track irregularity in this study.

The PSD of Sato track irregularity, which has been widely used in the study of high frequency vibration of track structure and wheel-rail noise generation, is used to simulate the short wavelength (less than 1 m) random track irregularity in this study. The expression of the PSD of Sato track irregularity (Sato, 1977) is as follow:

$$S(\Omega) = \frac{A}{\Omega^3} \tag{4}$$

where $S(\Omega)$ is the power spectral density, Ω is the spatial frequency in rad/m, and A is the roughness constant with values between 4.15×10^{-8} m.rad and 5.0×10^{-7} m.rad. In reference (Xu, 2004), a study was conducted to determine the roughness constant of the PSD of Sato track irregularity according to the rolling noise measured near the slab track of the Qinshen dedicated passenger line in China, and the value of the roughness constant proposed was 3.15×10^{-7} m.rad, which is used in the present study.

The method described in reference (Chen and Zhai, 1999) is used for the generation of sample waves in time series according to the expression of the PSD of track irregularity. The detailed procedures are as follows:

Firstly, the expression of $S(\Omega)$ is converted to $F(f)$ from the spatial frequency to the time frequency according to the following equation.

$$\Omega = \frac{2\pi f}{V} \tag{5}$$

where f is the time frequency in Hz, V is the speed of train.

Then, according to the required interval of time series samples dx and the total length of time series samples L, the total number of samples $N = L/dx$ and the interval of time frequency $\Delta f = V/L$ can be determined.

Thirdly, according to the required miminum wavelength $\lambda_{\min}$ and the maximum wavelength $\lambda_{\max}$, $f_{\min} = V/\lambda_{\max}$ and $f_{\max} = V/\lambda_{\min}$ in the time frequency can be determined.

Fourthly, according to the converted expression of $F(f)$, the discrete frequency sprecrum $X(n)$, $(n = 0,1,.....,N-1)$ can be determined as follow.

$$X(n)=\begin{cases}0 & n\times\Delta f\le f_{\min}\\ F(n\times\Delta f) & f_{\min}<n\times\Delta f<f_{\max}\\ 0 & n\times\Delta f\ge f_{\max}\end{cases} \tag{6}$$

At last, the sample waves in time series $Y(n)$ can be obtained by inverse Fourier transform as follow:

$$Y(n)=\sum_{n=0}^{N-1}\sqrt{2X(n)\Delta f}\exp(i\varphi_n) \tag{7}$$

where φ_n is a random phase angle uniformly distributed from 0 to 2π.

To consider both middle to long and short wavelength random track irregularities in the simulation, firstly, the samples according to the PSD of Sato track irregularity and American Class 6 track irregularity are generated respectively. Then the combined sample is generated by adding each amplitude of two samples whose coordinate is the same. The procedure can be seen in Figure 6.

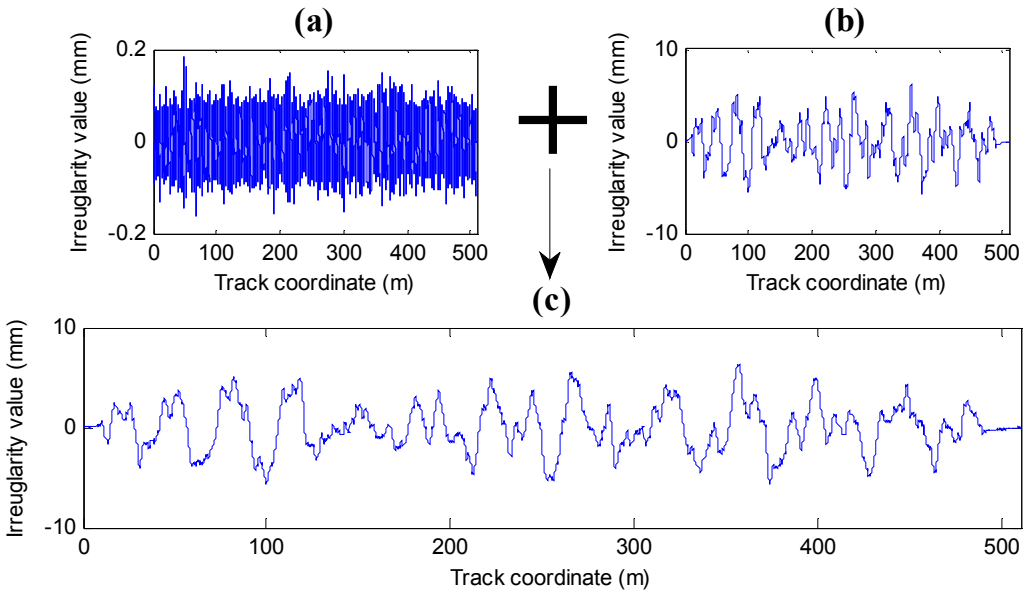

Figure 6: (a) Samples of the short wavelength random track irregularity. (b) Middle to long wavelength random track irregularity. (c) Combined random track irregularity.

3 VIBRATION EQUATIONS OF THE COUPLING DYNAMIC SYSTEM

Using the principle of total potential energy with the stationary value in elastic system dynamics presented by Zeng (2000), also seeing the reference (Lou and Zeng, 2005), one can derive the vibration equation of the subway train-SSFST-tunnel coupling dynamic model. The equation can be written in matrix form as follow:

$$\begin{bmatrix} M_{vv} & 0 \\ 0 & M_{tt} \end{bmatrix} \begin{Bmatrix} \ddot{X}_v \\ \ddot{X}_t \end{Bmatrix} + \begin{bmatrix} C_{vv} & 0 \\ 0 & C_{tt} \end{bmatrix} \begin{Bmatrix} \dot{X}_v \\ \dot{X}_t \end{Bmatrix} + \begin{bmatrix} K_{vv} & 0 \\ 0 & K_{tt} \end{bmatrix} \begin{Bmatrix} X_v \\ X_t \end{Bmatrix} = \begin{Bmatrix} F_{vg} + F_{vi} \\ F_{ti} \end{Bmatrix} \tag{8}$$

where, $\ddot{X}_{\mathrm{v}}$, $\dot{X}_{\mathrm{v}}$, and X_{v} denote the acceleration, velocity, and displacement vectors for the DOFs of the subway train sub-system, respectively; $\ddot{X}_{\mathrm{t}}$, $\dot{X}_{\mathrm{t}}$, and X_{t} denote the acceleration, velocity, and displacement vectors for the DOFs of the SSFST-tunnel sub-system, respectively; M_{vv}, C_{vv}, and K_{vv} denote the mass, damping, and stiffness matrices of the subway train sub-system, respectively; M_{tt}, C_{tt}, and K_{tt} denote the mass, damping, and stiffness matrices of the SSFST-tunnel sub-system, respectively; F_{vg} denotes the gravity sub-load vector of the subway train sub-system; F_{vi} and F_{ti} denote the sub-load vector of the wheel-rail interaction forces on subway train sub-system and SSFST-tunnel sub-system, respectively.

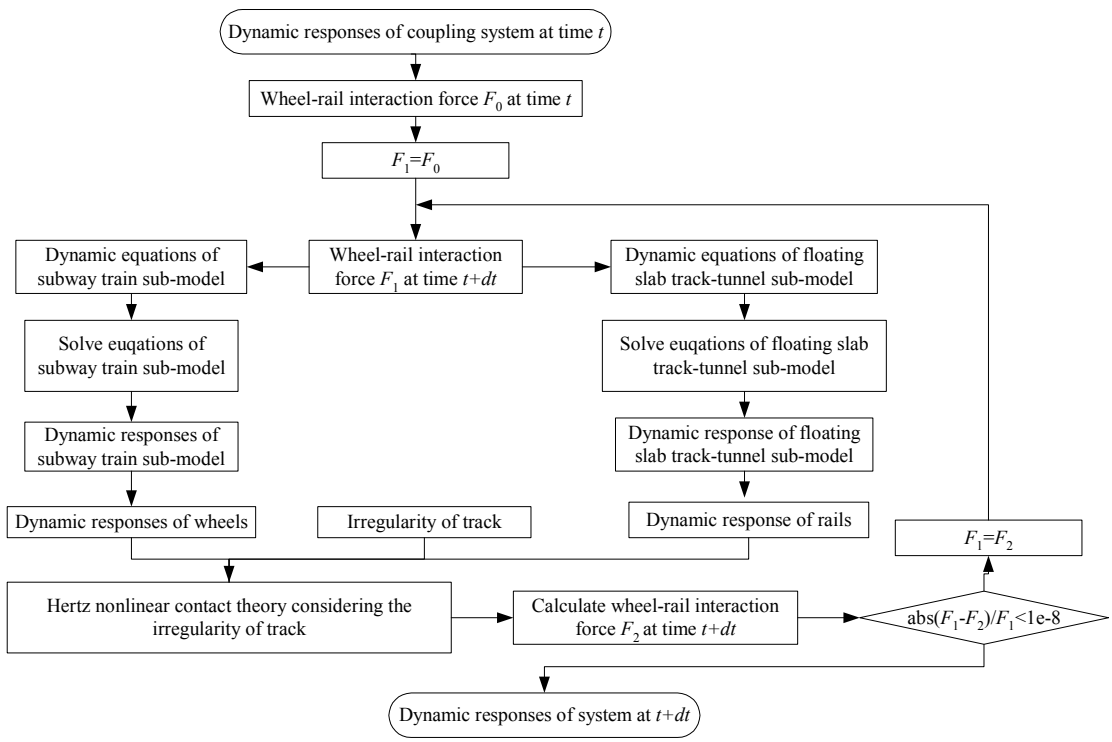

Figure 7: Flow-chart of the iteration procedures.

The vehicle differential equations can be found in the reference (Zhai and Cai, 1997). The detailed expressions of the stiffness matrix, mass matrix, damping matrix, and load vector of a single vehicle of the train sub-model can be found in the reference (Lei and Noda, 2002). Similar procedures for obtaining the stiffness matrix, mass matrix, damping matrix, and load vector of the SSFST-tunnel sub-system can be found in the reference (Lou, 2007). Solution procedures for the vibration equation of the coupled system are as follows.

(1) At time $t = 0$, the static displacement of the coupled system under the gravity load of vehicles and track irregularity is calculated and used as the initial value for the dynamic coupled system.

(2) When time $t > 0$, using the wheel-rail interaction model considering the track irregularity (Eq. 1) and an iteration procedure as described in Figure 7, the displacement, velocity, and acceleration of each DOFs of the coupled system, as well as the interaction forces between wheels and rails are calculated. Then, the force of each spring-damping element and the bending moment of each beam element can also be calculated. It should be mentioned that the convergence of the wheel-rail interaction force must be ensured during each time step.

4 POST-PROCESSING OF RESULTS

4.1 Calculation of maximum response for each component of the SSFST-tunnel sub-model

There are many nodes and elements for each component of the SSFST-tunnel sub-model, such as rails, fasteners, slabs, steel springs, and tunnels. For each component, the response of each different node (element) is different. To obtain the maximum response for each component of the system, the maximum response value and the corresponding node (element) number for each component are calculated and stored in the computer memory during each time step. Thus, the maximum response value and the corresponding node (element) number for each component can be obtained when the simulation is completed.

4.2 Obtaining and outputting the time history of the node (element) with the largest response for each component

On the one hand, more than 60000 time steps with the fixed step size are used in the calculations for each of the cases considered. On the other hand, the total number of nodes and elements of the coupled system exceeds 10000. Therefore, the complete time history for all nodes and elements can not be stored in the computer memory because the memory volume is limited in a personal computer.

In order to obtain the time history of the node (element) number with the largest response for each component of the steel spring-FST-tunnel sub-model, the simulation program must be run twice. The first run is used to obtain the node (element) number whose response is the largest (see Section 4.1), and the second run stores the time history of that node (element) with the largest response in the computer memory during the second simulation, and outputs it to the hard disk when the second simulation run is completed.

5 VALIDATION OF THE MODEL AND SELF-COMPILED COMPUTER PROGRAM

With the use of a self-compiled computer program, which is developed by MATLAB programming to calculate the train-track coupling dynamics, the dynamic responses of the coupled system are calculated for a subway train consisting of six identical vehicles (referred to as a B-type in this study) running on a SSFST in a tunnel at a speed of 60 km/h. The parameters for the B-type subway train and those of the SSFST-tunnel sub-model are listed in Tables 2 and 3, respectively. Both middle to long and short wavelength random track irregularities are considered. The sample used in this study is shown in Figure 6c.

Parameter	Unit	Value
Mass of car body	kg	43000
Mass of bogie	kg	3600
Mass of wheelset	kg	1900
Pitch inertia of car body	$kg.m^2$	1400000
Pitch inertia of bogie	$kg.m^2$	2320
Vertical damping of primary suspension	$N.s.m^{-1}$	30000
Vertical stiffness of primary suspension	$N.m^{-1}$	1400000
Vertical damping of secondary suspension	$N.s.m^{-1}$	50000
Vertical stiffness of secondary suspension	$N.m^{-1}$	580000
Wheelbase	m	2.3
Distance between center of front bogie and center of rear bogie	m	12.6
Total length of each vehicle	m	19

Table 2: Parameters for the B-type subway train.

Parameter	Unit	Value
Section area of rail	cm^2	77.45
Inertia moment of rail	cm^4	3217
Density of rail	$kg.m^{-3}$	7800
Elastic modulus of rail	GPa	210
Spacing of fastener	m	0.625
Vertical stiffness of fastener	$kN.mm^{-1}$	50
Damping of fastener	$kN.s.m^{-1}$	20
Width of slab	m	3
Thickness of slab	m	0.4
Elastic modulus of slab	GPa	36
Density of slab	$kg.m^{-3}$	2500
Stiffness of steel spring	$kN.mm^{-1}$	6.9
Section area of tunnel	m^2	5.4
Inertia moment of tunnel cross-section	m^4	44
Density of tunnel	$kg.m^{-3}$	2500
Modulus of tunnel foundation	MPa	300
Equivalent Winkler foundation stiffness of tunnel	MPa	60

Table 3: Parameters for the SSFST-tunnel sub-model.

Slab length is 30 m. As shown in Figure 2, the distance between the left end of the track and the head wheel of the train is 150 m at the starting time, and the train moves a distance of 330 m. The distance the train advances at each time step is 0.005 m, which is shorter than the half wavelength of the minimum short wavelength required. The total number of time steps for each case is 66000.

In order to evaluate the practical vibration reduction effect of SSFST in tunnel, in-situ metro-induced vibration tests were performed with the highly sensitive acceleration sensors in FST section in tunnel of Beijing metro line 5 (Li et al, 2011). The position of the installed accelerometer on the slab is 0.65m away from the rail towards the tunnel direction, and the position of the installed accelerometer on the tunnel wall is 1.5m above the top surface of slab.

The in-situ measured acceleration histories of the slab and tunnel are shown in Figure 8a and Figure 8b, respectively. The direction of the measured acceleration is upward. The corresponding acceleration histories of the slab and tunnel calculated by the self-compiled computer program are shown in Figure 9a and Figure 9b, respectively.

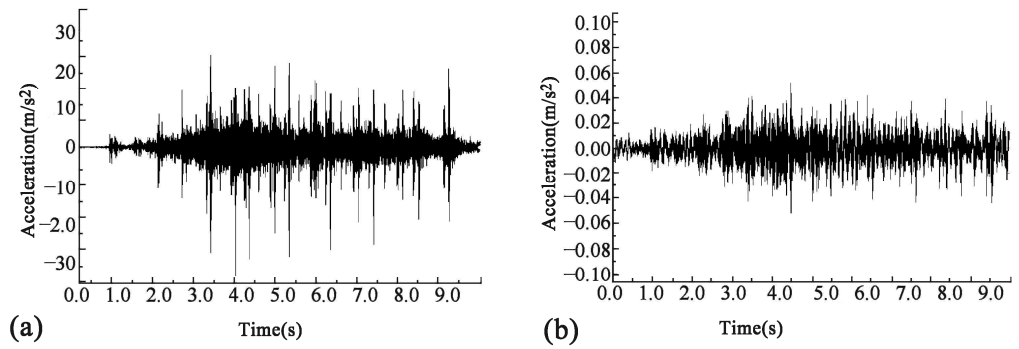

Figure 8: In-situ measured acceleration histories of the slab (a) and tunnel (b).

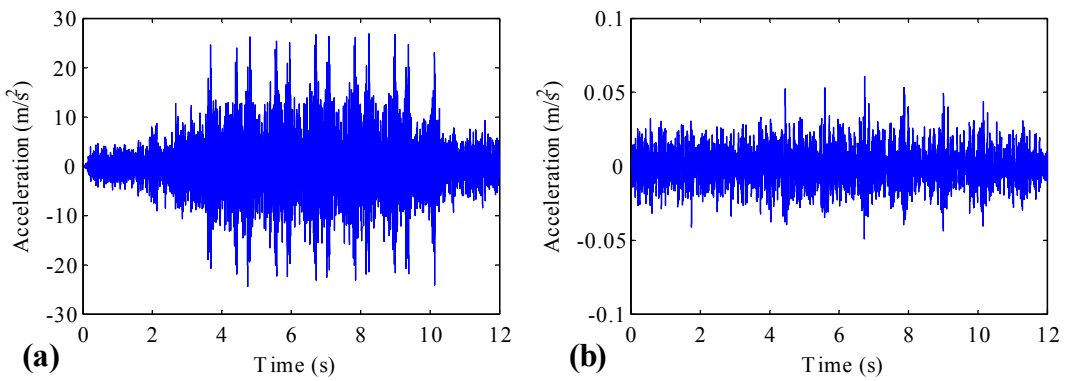

Figure 9: Calculated acceleration histories of the slab (a) and tunnel (b).

From Figure 8 and Figure 9, it can be seen that although the results calculated by the self-compiled computer program and those measured in-situ are not completely in accordance with each other, they are still in agreement to some extent. The discrepancies between the results are reasonable. The reasons are that there is a discrepancy between the random track irregularity used in this study and that of the in-situ measurements, and that the results shown in Figure 8a and Figure 8b were not the original results but were derived from filtered data. The example validates the correctness of the model and the self-compiled computer program.

6 CASE STUDIES

6.1 Calculation parameters

To comprehensively evaluate the influence of slab length on the dynamic characteristics of the coupled system under different track irregularity conditions and train speeds, 60 cases are studied. Slab lengths for cases 1-10 are 3.75 m, 5.625 m, 7.5 m, 11.25 m, 15 m, 18.75 m, 22.5 m, 26.25 m, 30 m, and 60 m, respectively. Slab lengths for per 10 cases, (i.e. cases 11-20, 21-30, 31-40, 41-50, and 51-60) are the same as those for cases 1-10, respectively. Subway train speeds for cases 1-20, 21-40, and 41-60 are 40km/h, 60km/h, and 90km/h respectively. Track irregularity condition for cases 1-10, 21-30, and 41-50 are smooth track without irregularity, and track irregularity condition for cases 11-20, 31-40, and 51-60 are uneven track with random track irregularity.

Except the slab length, subway train speed, and track irregularity condition, the other parameters are the same as those in Section 5.

6.2 Results and discussion

The relationships between the slab length and maximum dynamic response of each component of the coupled system for different train speeds and track irregularity conditions are shown in Figure 10-23. The acceleration time history and frequency distribution of wheelset, bogie, car body, rail, slab, and tunnel for Case 39, in which subway train runs along rail with random track irregularity supported by SSFST whose slab length is 30m at speed of 60km/h, are shown in Figure 24-Figure 30, respectively.

It should be mentioned that Figure 28a plots the time history of the rail node with the largest peak acceleration among all rail nodes. Similarly, Figure 29a and Figure 30a plot the time histories of the slab node and tunnel node with the largest peak acceleration among all slab nodes and all tunnel nodes, respectively. The detailed procedures by which the time history of the node with the largest response is obtained are described in Section 4.2.

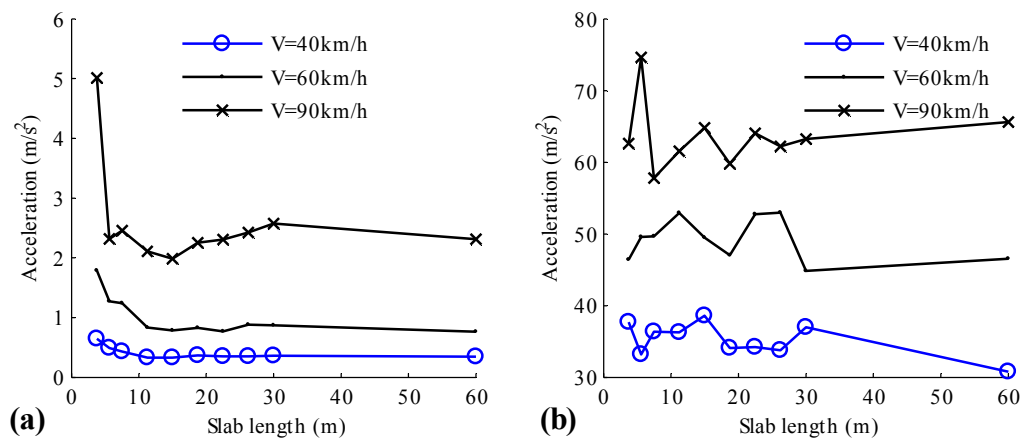

Figure 10: Relationship between slab length and maximum vertical acceleration of the front wheel of the first vehicle at different train speeds for cases (a) without irregularity and (b) with irregularity.

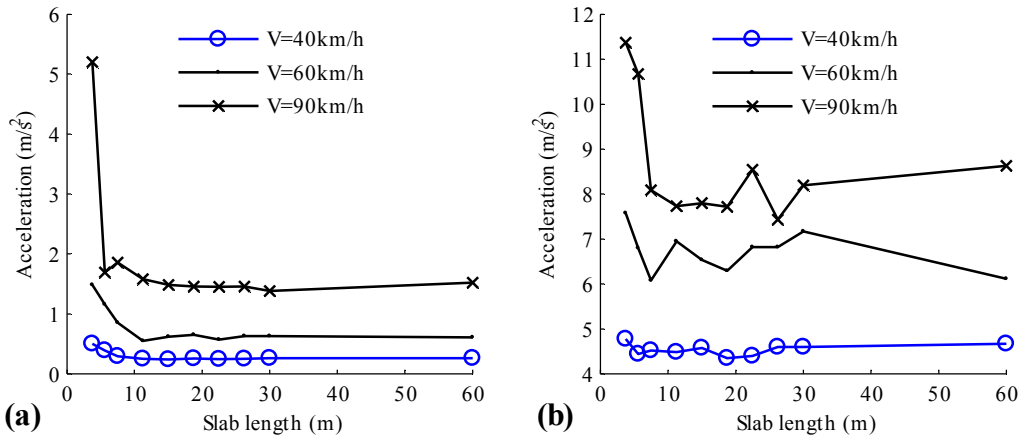

Figure 11: Relationship between slab length and maximum vertical acceleration of the front bogie of the first vehicle at different train speeds for cases (a) without irregularity and (b) with irregularity.

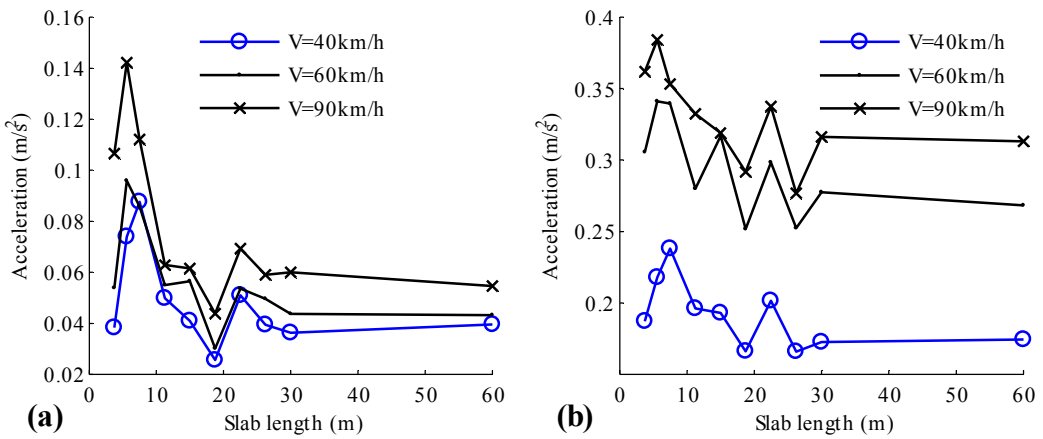

Figure 12: Relationship between slab length and maximum vertical acceleration of the first car body at the middle of the vehicle at different train speeds for cases (a) without irregularity and (b) with irregularity.

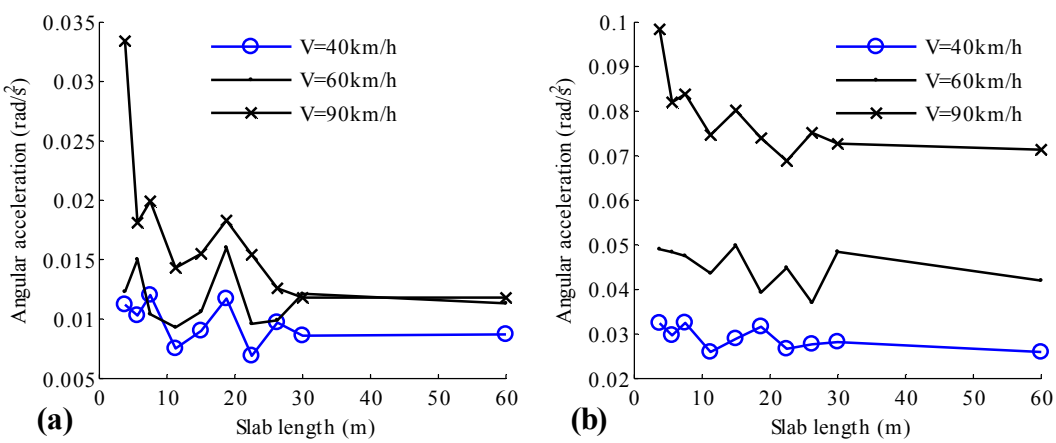

Figure 13: Relationship between slab length and maximum angular acceleration of the first car body at different train speeds for cases (a) without irregularity and (b) with irregularity.

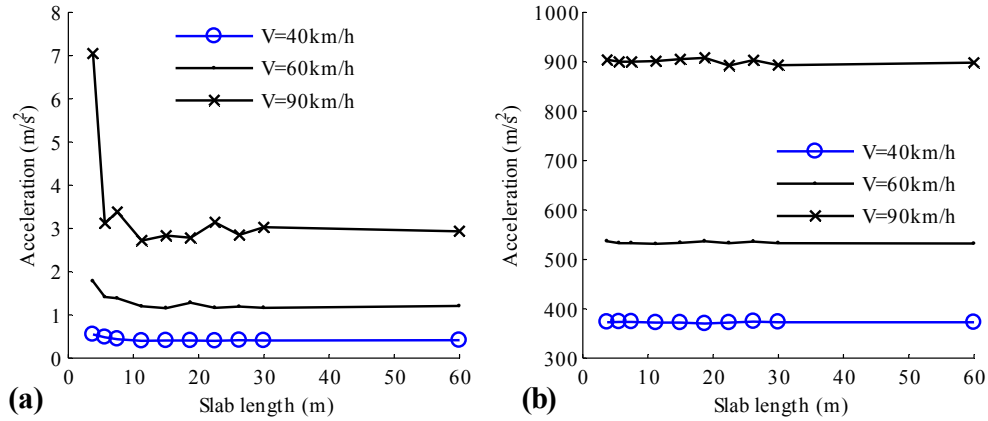

Figure 14: Relationship between slab length and maximum acceleration of rail at different train speeds for cases (a) without irregularity and (b) with irregularity.

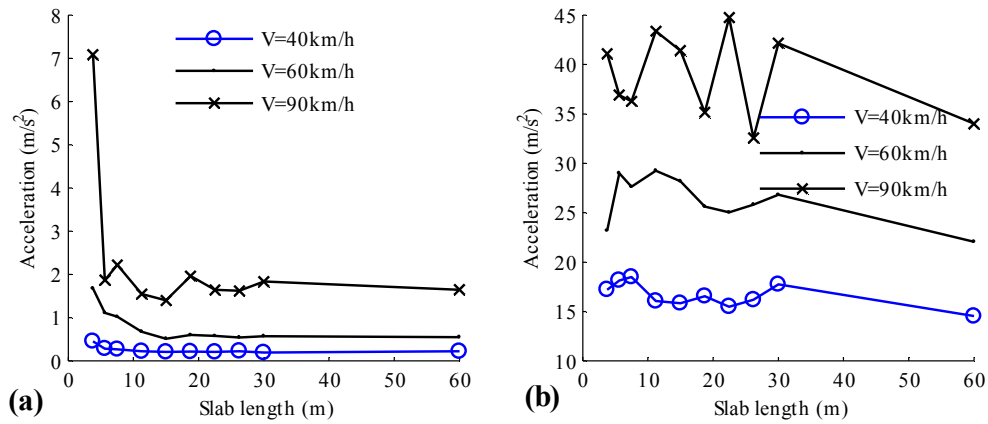

Figure 15: Relationship between slab length and maximum acceleration of slab at different train speeds for cases (a) without irregularity and (b) with irregularity.

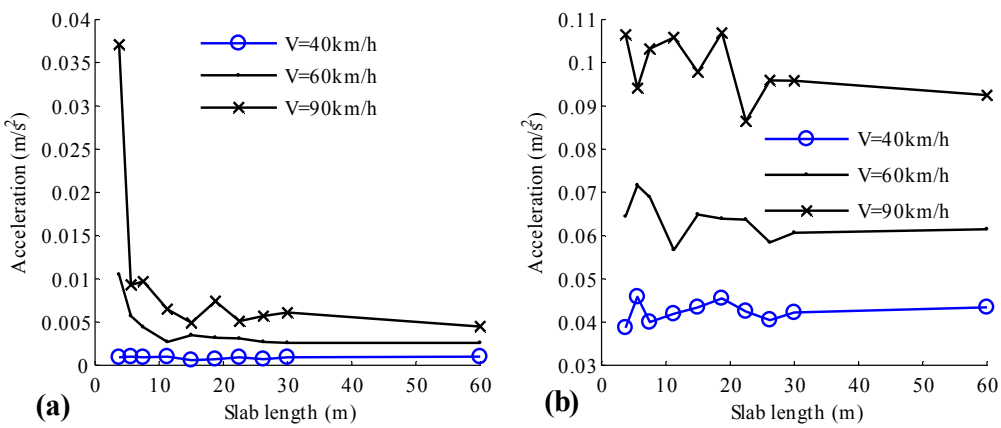

Figure 16: Relationship between slab length and maximum acceleration of tunnel at different train speeds for cases (a) without irregularity and (b) with irregularity.

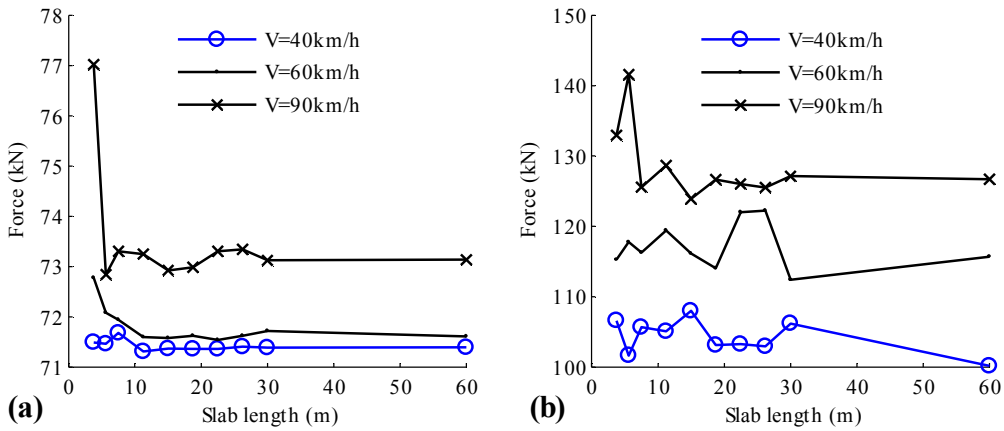

Figure 17: Relationship between slab length and maximum vertical wheel-rail force between the front wheel of first vehicle and the rail at different train speeds for cases (a) without irregularity and (b) with irregularity.

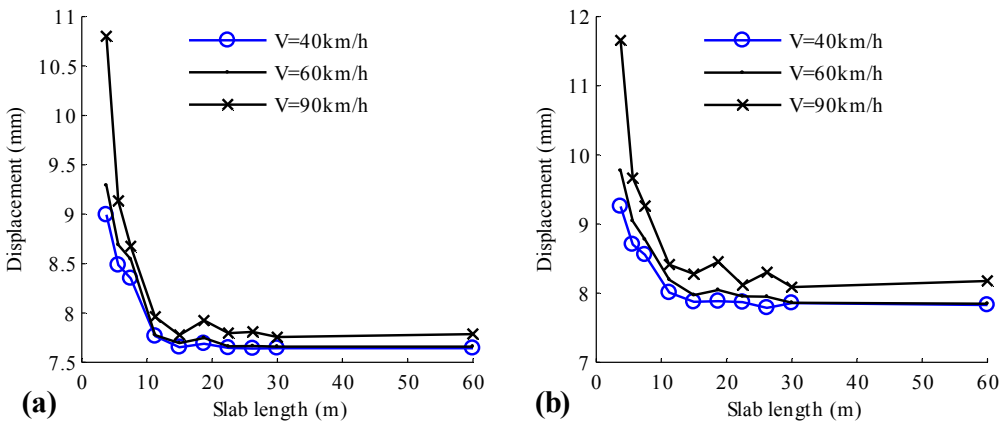

Figure 18: Relationship between slab length and maximum displacement of rail at different train speeds for cases (a) without irregularity and (b) with irregularity.

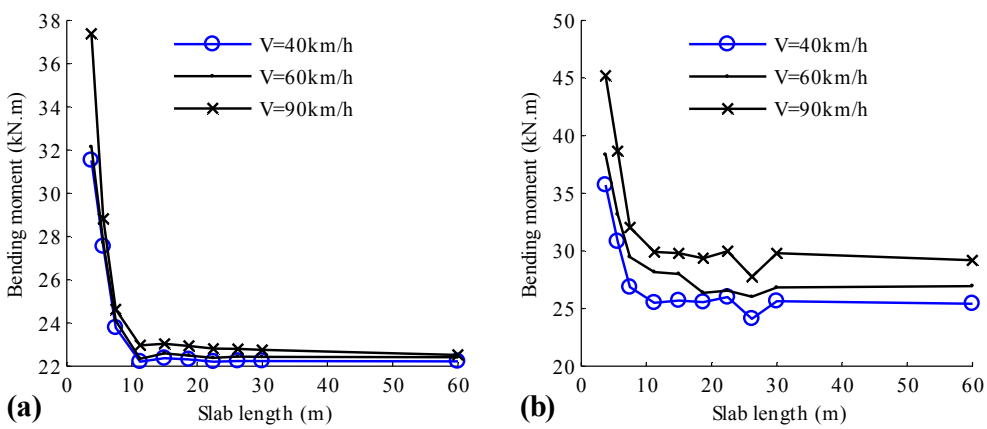

Figure 19: Relationship between slab length and maximum bending moment of rail at different train speeds for cases (a) without irregularity and (b) with irregularity.

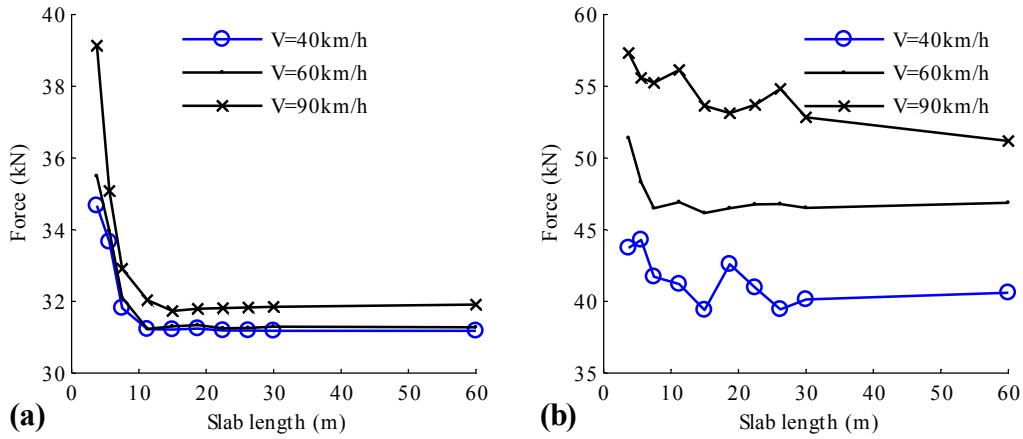

Figure 20: Relationship between slab length and maximum pressure force of fastener at different train speeds for cases (a) without irregularity and (b) with irregularity.

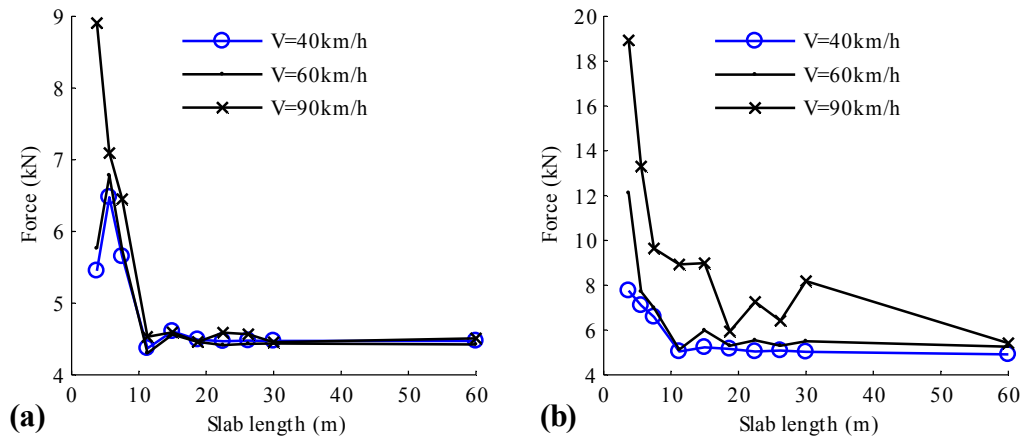

Figure 21: Relationship between slab length and maximum tensile force of fastener at different train speeds for cases (a) without irregularity and (b) with irregularity.

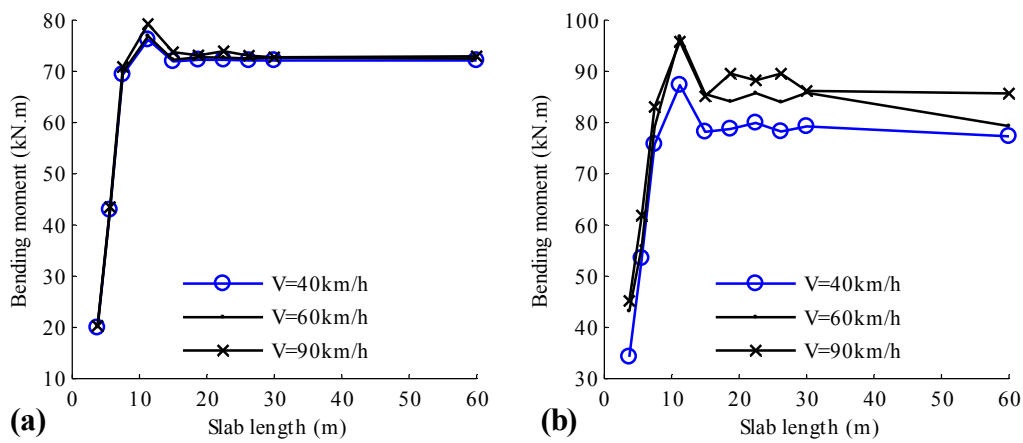

Figure 22: Relationship between slab length and maximum longitudinal bending moment of slab at different train speeds for cases (a) without irregularity and (b) with irregularity.

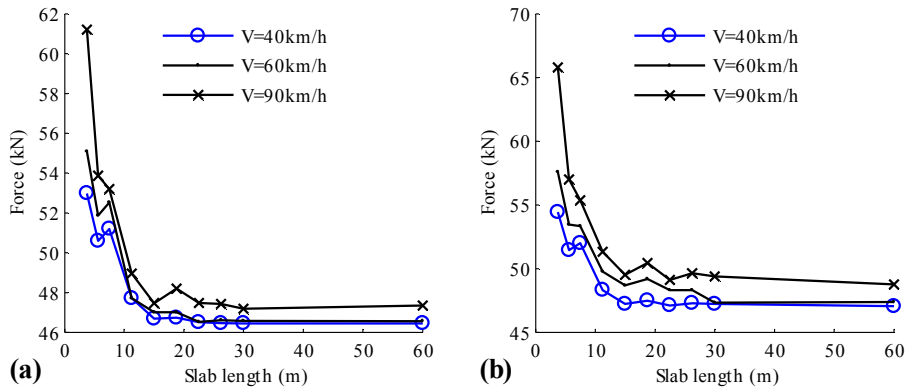

Figure 23: Relationship between slab length and maximum vertical force of steel spring at different train speeds for cases (a) without irregularity and (b) with irregularity.

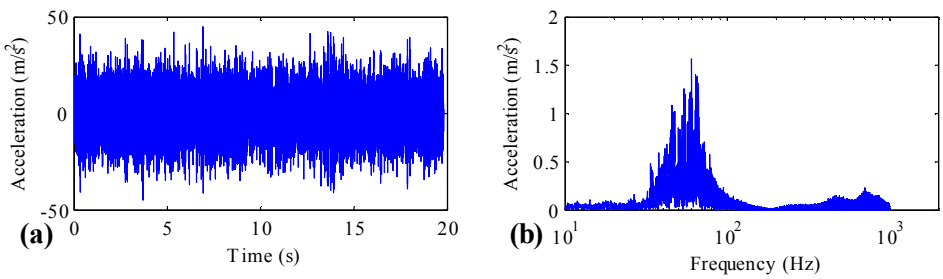

Figure 24: Time history (a) and frequency distribution (b) of acceleration of the front wheel of the first vehicle for Case 39.

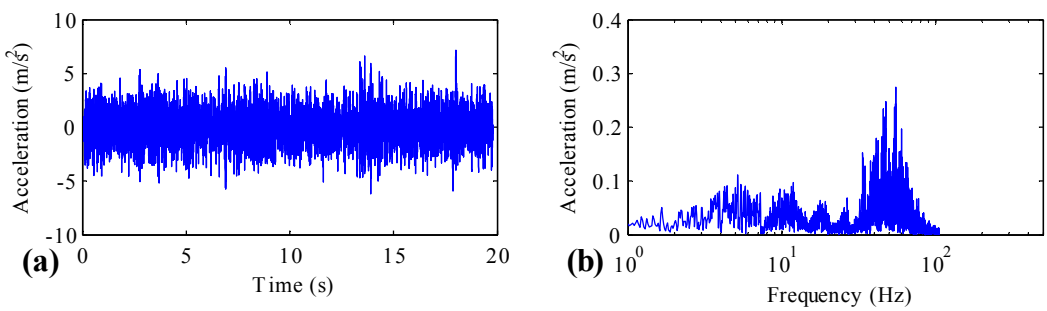

Figure 25: Time history (a) and frequency distribution (b) of acceleration of the front bogie of the first vehicle for Case 39.

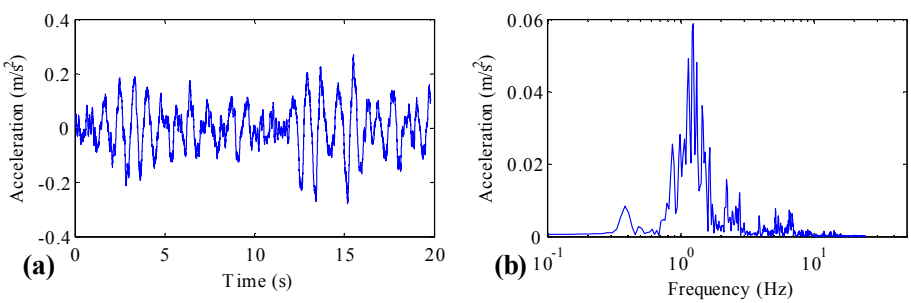

Figure 26: Time history (a) and frequency distribution (b) of acceleration of the car body at the middle point of first vehicle for Case 39.

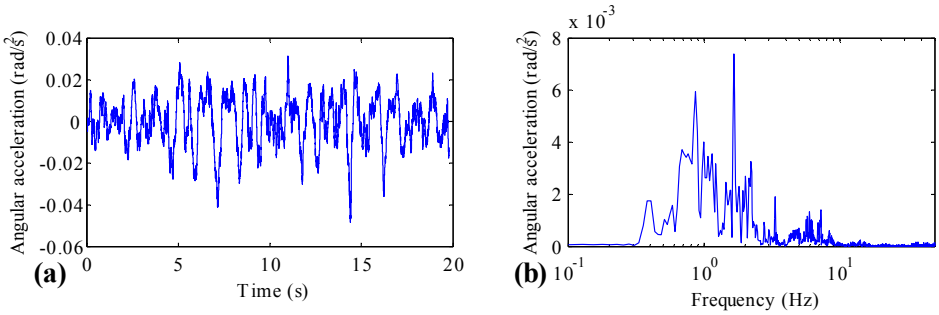

Figure 27: Time history (a) and frequency distribution (b) of angular acceleration of the car body of the first vehicle for Case 39.

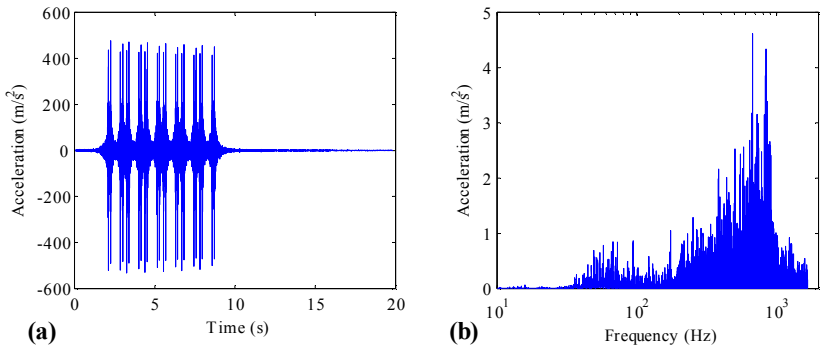

Figure 28: Time history (a) and frequency distribution (b) of acceleration of the rail for Case 39.

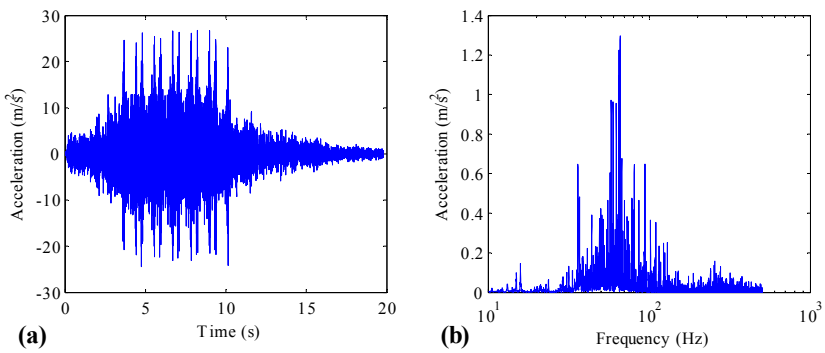

Figure 29: Time history (a) and frequency distribution (b) of acceleration of the slab for Case 39.

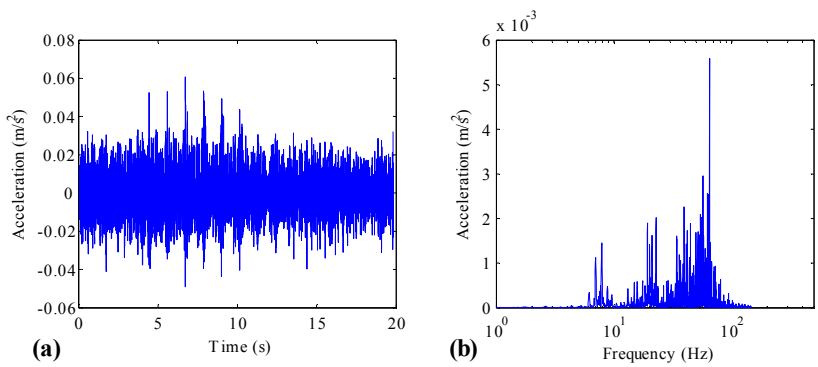

Figure 30: Time history (a) and frequency distribution (b) of acceleration of the tunnel for Case 39.

From Figure 10-30, the following points can be observed:

(1) It can be seen from Figure 10a, 11a, 14a, 15a, and 16a that although the accelerations of wheelset, bogie, rail, slab, and tunnel do not change monotonically with the increase of slab length under the smooth track condition, the overall rule is quite obvious, that is, the shorter the slab length is, the larger the acceleration is. Acceleration changes little when the slab length exceeds the distance between two bogies of a vehicle (12.6 m in this study).

(2) It can be seen from Figure 12a and Figure 13a that the vertical acceleration and angular acceleration of car body do not change monotonically with the increase of slab length under the smooth track condition, and there are many fluctuations when slab length is less than 22.5m. Although the influence law of slab length on the dynamic responses of car body is very complex, it still can be seen from Figure 12a and Figure 13a that when the slab length is around 11.25m, the vertical acceleration and angular acceleration of car body are relatively small and they change little when the slab length exceeds 22.5m.

(3) As is clear from Figure 10-16, the random track irregularity has substantial influence on the vibration acceleration of wheelset, bogie, car body, rail, slab, and tunnel. For example, the maximum vertical acceleration of the rail under the random track irregularity condition is about several hundred times of that under the perfectly smooth track condition. The maximum vertical acceleration of the first car body under the random track irregularity condition is about 2.7-8.3 times of that under the perfectly smooth track condition.

(4) From Figure 10-16, it can be seen that the influence of the slab length on the vibration acceleration of wheelset, bogie, car body, rail, slab, and tunnel under the random track irregularity condition varies. It is closely related to the dominant frequency distribution of the vibration acceleration of the components of the coupled system (Figures 24b-30b). Generally speaking, the lower the dominant frequency distribution of the vibration acceleration of the components of the coupled system is, the greater the influence of the slab length is. The main reason for this condition is that the excitation frequency caused by the moving train at a constant speed v passing slab length L is v/L, whose value is low under the normal operation condition of the subway train, so the slab length has greater influence on the vibration acceleration of the coupled system whose dominant frequency is low.

Because the dominant frequency distribution of the acceleration of the bogie, wheel, rail, slab, and tunnel is relatively higher than the slab passing frequency, the vibration acceleration of the bogie, wheel, rail, slab, and tunnel are affected far more by the random track irregularity than by the slab length. The maximum acceleration of the bogie, wheel, rail, slab, and tunnel does not necessarily appear in the short length FST. However, because the dominant frequency distribution of the acceleration of the car body is relatively low, the slab length has greater influence on the vibration acceleration of the car body than that of the bogie, wheel, rail, slab, and tunnel. The maximum acceleration of the car body tends to become smaller with increasing slab length, although there are some fluctuations because of the influence of random track irregularity.

(5) From Figure 14b, it is clear that the wheel-rail force variation is very small and it is negligible under the perfectly smooth track condition for train speed under 60km/h. And it is also negligible under the perfectly smooth track condition for train speed at 90km/h when slab length is longer than 5m. However, the influence of slab length on the wheel-rail interaction force under the random track irregularity condition is complex. The maximum wheel-rail interaction force

does not necessarily appear in the short length FST because of the large influence of random track irregularity.

(6) It is apparent from Figure 18 that slab length has obvious influence on the maximum vertical displacement of the rail. The maximum vertical displacement of the rail decreases by about 20% with increasing slab length for train speed under 60km/h, and decreases by about 30% for train speed at 90km/h.

The reason for the reduction is that the force of the steel spring under the slab is relatively uniform and the displacement of the steel spring under the slab is relatively small when the slab length is long.

The reason for higher reduction rate of the maximum vertical displacement of the rail for higher subway train speed is that the influence of slab length on dynamic force of fastener and steel spring which are the main causes of deformation of the track, is much larger when train speed is higher, as shown in Figures 20-21 and Figure 23.

(7) It is evident from Figure 19 that slab length has significant influence on the bending moment of the rail. The maximum moment of the rail decreases by about 30% with increasing slab length for lower train speed under 60km/h, and decreases by about 35-40% for train speed at 90km/h.

The reason for the reduction is that the local deformation of the rail near the ends of two adjacent slabs is relatively small when the slab length is long. Thus, the bending moment of the rail is relatively small with increasing slab length.

The larger reduction rate of the bending moment of the rail for higher subway train speed is due to the larger influence of slab length on dynamic wheel-rail force as shown in Figure 17 and dynamic force of fastener as shown in Figure 20-21, which are closely related to the bending moment of rail.

(8) It is clear from Figure 20-21 that slab length has some influence on the fastener force. The maximum pressure force of the fastener decreases by about 7-19% and the maximum tensile force of the fastener decreases by about 17-71% with increasing slab length for different irregularity track conditions and train speeds. The reduction rate is closely related to the subway train speed. The higher subway train speed is , the larger reduction rate will be.

The reason for the reduction is similar to that of the bending moment of rail. The local deformation of the slab is relatively small when the slab length is long.

The reduction rate of the maximum tensile force of the fastener is much larger than that of the maximum pressure force. The reason is that the pressure force of the fastener is influenced mainly by the gravity load of the vehicle and random track irregularity rather than by slab length, while the tensile force of the fastener is closely related to the local deformation of the track near the ends of two adjacent slabs, which bears a close relationship with slab length.

The reason for larger reduction rate of preesure and tensile fastener force for higher subway train speed is due to the larger influence of slab length on dynamic response of rail and slab which are closely related to the fastener preesure and tensile force.

(9) From Figure 22, we can conclude that slab length has substantial influence on the longitudinal bending moment of the slab. The maximum longitudinal bending moment of the slab increases substantially and it is almost doubled with an increase of slab length at first. Then it be-

gins to drop slightly. And the maximum longitudinal bending moment of the slab changes little when the slab length exceeds the distance between two bogies of a vehicle.

The main reason is that when the slab length is short, the bending stiffness of the slab is very high and the slab acts as a rigid body under the train load, resulting in a small longitudinal bending moment of the slab. With an increase of slab length, the bending stiffness of the slab reduces and the slab acts as a flexible beam under the train load. Therefore, the maximum longitudinal bending moment of the slab increases substantially with increasing slab length at first.

Besides the bending stiffness of the slab, the longitudinal bending moment is also related to the force of the steel spring which decreases with increasing slab length; therefore, the longitudinal bending moment drops slightly when the slab length exceeds some value. The force of the steel spring is nearly constant when the slab length exceeds the distance between two bogies of a vehicle, so the longitudinal bending moment of the slab changes little when the slab length exceeds the distance between the two bogies of a vehicle.

(10) As is apparent from Figure 23, the slab length has large influence on the maximum vertical force of the steel spring. The maximum vertical force of the steel spring decreases by about 12-25% with an increase of slab length for different irregularity track conditions and train speeds. The force of the steel spring is nearly constant when the slab length exceeds the distance between two bogies of a vehicle.

The reason for the reduction is that the local deformation of the slab near the ends of two adjacent slabs is relatively large when the slab length is short, so the steel spring near the ends of two adjacent slabs of shorter length bears more pressure forces.

The reason for larger reduction rate of steel spring force for higher subway train speed is due to the larger influence of slab length on dynamic response of the slab and the force acting on the slab, which are closely related to the steel spring force.

7 CONCLUSIONS AND RECOMMENDATIONS

A subway train-SSFST-tunnel coupling dynamic model considering short and middle to long wavelength random track irregularities, as well as longitudinal connection between adjacent slabs of SSFST, is developed. Based on this model, the influence of slab length on dynamic characteristics of the system under different track irregularity conditions and train speeds is theoretically studied. The following conclusions can be obtained:

(1) In general, under the perfectly smooth track condition, the dynamic performance of the bogie, wheel, rail, slab, and tunnel is improved with increasing slab length, although vibration accelerations of these components do not decrease monotonically with increasing slab length. The influence of slab length on dynamic performance of the car body is more complex than other components of the coupled system. There are still some influence laws that the vertical acceleration and angular acceleration of car body are relatively small when the slab length is around 11.25m and they change little when the slab length exceeds 22.5m.

(2) Slab length has varying influence on the vibration acceleration of the subway train-SSFST-tunnel coupled system under the random track irregularity condition. Generally speaking, the lower the dominant frequency distribution of the vibration acceleration is, the greater the influence of slab length is. The maximum bogie acceleration, wheel acceleration, rail acceleration, slab

acceleration, and tunnel acceleration do not necessarily appear in the short length FST because of the significant influence of random track irregularity. The maximum acceleration of the car body tends to become smaller with increasing slab length, although there are small fluctuations because of the influence of track irregularity.

(3) Slab length has significant impact on the force of rail, fastener, and steel spring regardless of the track irregularity condition. With an increase of slab length, the force of rail, fastener, and steel spring also decreases significantly, which helps to lengthen the service life of these components. Slab length has significant influence on the dynamic force of rail, fastener, and steel spring when train speed is higher.

(4) Slab length has significant influence on the longitudinal bending moment of the slab regardless of track irregularity condition. The maximum longitudinal bending moment of the slab increases substantially and is almost doubled with an increase of slab length at first, then it begins to drop slightly, and the maximum longitudinal bending moment of the slab changes little when the slab length exceeds the distance between two bogies of a vehicle. Some effective measures, such as increasing the height of the slab and using more steel bars in the slab, should be taken to improve the bending resistance capacity of long length slabs. Slab length has significant influence on the longitudinal bending moment of the slab when train speed is higher.

(5) Slab length around 11.25m or above 22.5m is recommended for underground SSFST when the operation speed of subway train is moderate. Slab length above 22.5m is recommended when the operation speed of subway train is very high.

Acknowledgments

The study is supported by the Natural Science Foundation of China (Nos. 51178469 and 51078360), the National Science Joint High Speed Railway Foundation of China (No. U1334203), and the State Scholarship Fund of China Scholarship Council (No. 201208430112).

References

Andersson, E., Berg, M., Stichel, S., (1998). Rail Vehicle Dynamics: Fundamentals and Guidelines. Royal Institute of Technology (KTH), Stockholm.

Au, F.T.K., Wang, J.J., Cheung, Y.K., (2002). Impact study of cable-stayed railway bridges with random rail irregularities. Engineering Structures 24(5): 529-541.

Auersch, L., (2012). Dynamic Behavior of Slab Tracks on Homogeneous and Layered Soils and the Reduction of Ground Vibration by Floating Slab Tracks. Journal of Engineering Mechanics 138(8): 923-933.

Bowe, C.J., Mullarkey, T.P., (2005). Wheel-rail contact elements incorporating irregularities. Advances in Engineering Software 36(11): 827-837.

Chen, G., Zhai, W.M., (1999). Numerical simulation of the stochastic process of railway track irregularities. Journal of Southwest Jiaotong University 34(2): 132-137 (in Chinese).

Cox, S.J., Wang, A., Morison, C., Carels, P., Kelly, R., Bewes, O.G., (2006). A test rig to investigate slab track structures for controlling ground vibration. Journal of Sound and Vibration 293(3): 901-909.

Ding, D.Y., Liu, W.N., Li, K.F., Sun, X.J., Liu, W.F., (2011). Low frequency vibration tests on a floating slab track in an underground laboratory. Journal of Zhejiang University SCIENCE A 12(5): 345-359 (in Chinese).

Dings, P.C., Dittrich, M.G., (1996). Roughness on Dutch railway wheels and rails. Journal of Sound and Vibration 193(1): 103-112.

Forrest, J.A., Hunt, H.E.M., (2006). Ground vibration generated by trains in underground tunnels. Journal of Sound and Vibration 294(4): 706-736.

Gardien, W., Stuit, H.G., (2003). Modelling of soil vibrations from railway tunnels. Journal of Sound and Vibration 267(3): 605-619.

Gupta, S., Degrande, G., (2010). Modelling of continuous and discontinuous floating slab tracks in a tunnel using a periodic approach. Journal of Sound and Vibration 329(8): 1101-1125.

Gupta, S., Hussein, M.F.M., Degrande, G., Hunt, H.E.M., Clouteau, D., (2007). A comparison of two numerical models for the prediction of vibrations from underground railway traffic. Soil Dynamics and Earthquake Engineering 27(7): 608-624.

Gupta, S., Liu, W.F., Degrande, G., Lombaert, G., Liu, W.N., (2008). Prediction of vibrations induced by underground railway traffic in Beijing. Journal of Sound and Vibration 310(3): 608-630.

Hamid, A., Yang, T.L., (1981). Analytical descriptions of track-geometry variations. Transportation Research Record 838: 19-26.

Hung, H.H., Chen, G.H., Yang, Y.B., (2013). Effect of railway roughness on soil vibrations due to moving trains by 2.5 D finite/infinite element approach. Engineering Structures 57: 254-266.

Hussein, M.F.M., Hunt, H.E.M., (2006). Modelling of floating-slab tracks with continuous slabs under oscillating moving loads. Journal of Sound and Vibration 297(1): 37-54.

Hussein, M.F.M., Hunt, H.E.M., (2009). A numerical model for calculating vibration due to a harmonic moving load on a floating-slab track with discontinuous slabs in an underground railway tunnel. Journal of Sound and Vibration 321(1): 363-374.

Iyengar, R.N., Jaiswal, O.R., (1995). Random field modeling of railway track irregularities. Journal of Transportation Engineering 121(4): 303-308.

Ju, S.H., Liao, J.R., Ye, Y.L., (2010). Behavior of ground vibrations induced by trains moving on embankments with rail roughness. Soil Dynamics and Earthquake Engineering 30(11): 1237-1249.

Kitagawa, T., Thompson, D.J., (2006). Comparison of wheel/rail noise radiation on Japanese railways using the TWINS model and microphone array measurements. Journal of Sound and Vibration 293(3): 496-509.

Kuo, C.M., Huang, C.H., Chen, Y.Y., (2008). Vibration characteristics of floating slab track. Journal of Sound and Vibration 317(3): 1017-1034.

Lei, X., Noda, N.A., (2002). Analyses of dynamic response of vehicle and track coupling system with random irregularity of track vertical profile. Journal of Sound and Vibration 258(1): 147-165.

Li, K.F., Liu, W.N., Sun, X.J., Ding, D.Y., Yuan, Y., (2011). In-situ Test of Vibration Attenuation of Underground Line of Beijing Metro Line 5. Journal of the China Railway Society 33(4): 112-118 (in Chinese).

Lombaert, G., Degrande, G., Vanhauwere, B., Vandeborght, B., François, S., (2006). The control of ground-borne vibrations from railway traffic by means of continuous floating slabs. Journal of Sound and Vibration 297(3): 946-961.

Lou, P., (2007). Finite element analysis for train–track–bridge interaction system. Archive of Applied Mechanics 77(10): 707-728.

Lou, P., Zeng, Q.Y., (2005). Formulation of equations of motion of finite element form for vehicle-track-bridge interaction system with two types of vehicle model. International Journal for Numerical Methods in Engineering 62(3): 435-474.

Müller, K., Grundmann, H., Lenz, S., (2008). Nonlinear interaction between a moving vehicle and a plate elastically mounted on a tunnel. Journal of Sound and Vibration 310(3): 558-586.

Sato, Y., (1977). Study on high-frequency vibrations in track operated with high-speed trains. Quarterly Reports of Railway Technical Research Institute 18(3): 109-114.

Saurenman, H., Phillips, J., (2006). In-service tests of the effectiveness of vibration control measures on the BART rail transit system. Journal of Sound and Vibration 293(3): 888-900.

Vogiatzis, K., (2012). Environmental ground borne noise and vibration protection of sensitive cultural receptors along the Athens Metro Extension to Piraeus. Science of the Total Environment 439: 230-237.

Wu, T.X., Thompson, D.J., (2000). Theoretical investigation of wheel/rail non-linear interaction due to roughness excitation. Vehicle System Dynamics 34(4): 261-282.

Xu, Z.S., (2004). Prediction and control of wheel/ rail noise for rail transit, Ph.D. Thesis (in Chinese), Southwest Jiaotong University, China.

Zeng, Q.Y., (2000). The principle of total potential energy with stationary value in elastic system dynamics. Journal of Huazhong University of Science and Technology 28(1): 1-3 (in Chinese).

Zhai, W., Cai, Z., (1997). Dynamic interaction between a lumped mass vehicle and a discretely supported continuous rail track. Computers & structures 63(5): 987-997.

Zhang, N., Xia, H., (2013). Dynamic analysis of coupled vehicle–bridge system based on inter-system iteration method. Computers & Structures 114: 26-34.